NeuroImage 186 (2019) 211–220

Contents lists available at ScienceDirect

NeuroImage

journal homepage: www.elsevier.com/locate/neuroimage

How do spatially distinct frequency specific MEG networks emerge from one underlying structural connectome? The role of the structural eigenmodes

Prejaas Tewarie [a,*], Romesh Abeysuriya [b], Áine Byrne [c,d], George C. O'Neill [a], Stamatios N. Sotiropoulos [e,f], Matthew J. Brookes [a], Stephen Coombes [c]

[a] Sir Peter Mansfield Imaging Centre, School of Physics and Astronomy, University of Nottingham, Nottingham, United Kingdom
[b] Oxford Centre for Human Brain Activity, Department of Psychiatry, University of Oxford, United Kingdom
[c] School of Mathematical Sciences, University of Nottingham, Nottingham, United Kingdom
[d] Center for Neural Science, New York University, United States
[e] Sir Peter Mansfield Imaging Centre, School of Medicine, University of Nottingham, United Kingdom
[f] FMRIB Centre, University of Oxford, United Kingdom

ARTICLE INFO

Keywords:
Functional connectivity
Magnetoencephalography
Neural mass
Neural mass bifurcation
Eigenmodes
MEG

ABSTRACT

Functional networks obtained from magnetoencephalography (MEG) from different frequency bands show distinct spatial patterns. It remains to be elucidated how distinct spatial patterns in MEG networks emerge given a single underlying structural network. Recent work has suggested that the eigenmodes of the structural network might serve as a basis set for functional network patterns in the case of functional MRI. Here, we take this notion further in the context of frequency band specific MEG networks. We show that a selected set of eigenmodes of the structural network can predict different frequency band specific networks in the resting state, ranging from delta (1–4 Hz) to the high gamma band (40–70 Hz). These predictions outperform predictions based from surrogate data, suggesting a genuine relationship between eigenmodes of the structural network and frequency specific MEG networks. We then show that the relevant set of eigenmodes can be excited in a network of neural mass models using linear stability analysis only by including delays. Excitation of an eigenmode in this context refers to a dynamic instability of a network steady state to a spatial pattern with a corresponding coherent temporal oscillation. Simulations verify the results from linear stability analysis and suggest that theta, alpha and beta band networks emerge very near to the bifurcation. The delta and gamma bands in the resting state emerges further away from the bifurcation. These results show for the first time how delayed interactions can excite the relevant set of eigenmodes that give rise to frequency specific functional connectivity patterns.

1. Introduction

It has been argued for several years that neuronal synchronisation is crucial to uphold human cognition. Neuronal synchronisation is widely studied in the context of networks, which can be obtained from various imaging modalities, such as magnetoencephalography (MEG) or the electroencephalogram (EEG). Temporal modulations in MEG networks are assumed to underlie cognitive processing in the brain (Bassett and Sporns, 2017; Bassett et al., 2011), while perturbations to these networks are presumed to lead to cognitive disturbance and physical disability in several neuropsychiatric disorders (Stam, 2014; Stam et al., 2014). The integrity of neuronal networks has also been studied in the context of the emergence of consciousness (Amico et al., 2017; Cavanna et al., 2017). Taken together, there is ample evidence for the pivotal role of neuronal networks in the human brain, however, there is a need to progress from a purely phenomenological description to an understanding of how neuronal networks emerge and the mechanisms that lead to empirically observed perturbations to these networks. This is particularly important for the interpretation of resting-state MEG data where there is no cognitive or sensorimotor context (or locking) during which the oscillations occur.

A conventional way to understand how functional networks are brought about is to assume that they emerge from the underlying structural network and dynamical properties of connected neuronal

* Corresponding author. Sir Peter Mansfield Imaging Centre, School of Physics and Astronomy, University of Nottingham, University Park, Nottingham, United Kingdom.
E-mail address: prejaas.tewarie@nottingham.ac.uk (P. Tewarie).

https://doi.org/10.1016/j.neuroimage.2018.10.079
Received 7 March 2018; Received in revised form 6 August 2018; Accepted 29 October 2018
Available online 3 November 2018

populations on top of this network (Ashwin et al., 2016; Coombes, 2010). Several approaches have been employed and the initial studies showed that functional networks are not merely a one-to-one reflection of the underlying structural network (Honey et al., 2009). Additional properties of the structural network that were important to explain this gap were the Euclidean distance between regions (Alexander-Bloch et al., 2012), the outer product of the structural degree sequence (Tewarie et al., 2014) and detours along the shortest paths in the structural network (Goñi et al., 2014). In recent years there has been a rise in studies aiming to formalise a mapping between structural and functional networks (Robinson, 2012; Meier et al., 2016; Saggio et al., 2016; Deco et al., 2014). Several groups have now independently demonstrated that functional networks can be understood in terms of a weighted sum of monosynaptic and polysynaptic walks in the underlying structural networks (Robinson, 2012; Meier et al., 2016; Bettinardi et al., 2017; Mehta-Pandejee et al., 2017).

However, most of these structure-function studies have been conducted by making use of resting-state fMRI data, whilst only a few have employed neurophysiological data (Deco et al., 2017; Garcés et al., 2016; Meier et al., 2016; Tewarie et al., 2014). Neurophysiological data boasts both a superior temporal and spectral resolution compared to fMRI data. However, this presents the added difficulty of explaining not one, but several frequency band specific, functional networks, which may also be evolving in time. The question that then arises, is how these different functional networks emerge from the same underlying structural network. A promising recent approach to understand the spatial features of resting state networks is to analyse them in terms of the eigenmodes of the structural connectivity (Atasoy et al., 2016; Gabay and Robinson, 2017; Robinson et al., 2016; Wang et al., 2017; Visser et al., 2017).

The aim of the current study is to analyse the role of the eigenmodes of the structural network in order to explain distinct frequency band specific networks. Using diffusion MRI and MEG data, we first analyse whether individual structural eigenmodes correspond to frequency specific MEG networks and in addition whether they can be regarded as a basis set for MEG networks. We then develop a network model comprised of connected Wilson-Cowan oscillators and using linear stability analysis we show how the excitation of a certain set of structural eigenmodes can explain frequency band specific functional networks. This is analysed with and without the inclusion of axonal conduction delays. Results from linear stability analysis are subsequently supported by simulations of Wilson-Cowan oscillator networks.

2. Methods

2.1. MEG: data acquisition and pre-processing

Resting-state MEG data were obtained from the Human Connectome Project (Van Essen et al., 2013) as part of the HCP MEG2 release. Briefly, data were collected on a whole-head Magnes 3600 scanner (4D Neuroimaging, San Diego, CA, USA) from 89 subjects (Larson-Prior et al., 2013; Van Essen et al., 2013); 95 subjects were included in the release, but resting-state recordings that passed the quality control checks (which included tests for excessive SQUID jumps, sensible power spectra and correlations between sensors, and for sufficiently many well-behaved recording channels) were not available from six. All subjects were young (22–35 years of age) and healthy. Resting state measurements were taken in three consecutive sessions for each subject with little or no break in between, for 6 min each. The data have been provided pre-processed (Larson-Prior et al., 2013), after passing through a pipeline to remove any artefactual segments of time from the recordings, identify any recording channels that are faulty, and to regress out artefacts which appear as independent components in an ICA decomposition with clear artefactual temporal signatures (such as eye-blinks or cardiac interference). Sensor-space data were down-sampled from 509 Hz to 300 Hz to facilitate processing, with the application of a zero-phase anti-aliasing filter.

2.2. MEG: source localisation

We performed additional processing steps for source localisation. An atlas-based beamforming approach was adopted to project MEG sensor level data into source-space (Hillebrand et al., 2012). The cortex was parcellated into 78 cortical regions according to the automated anatomical labelling (AAL) atlas (Tzourio-Mazoyer et al., 2002). This was done by registering each subject's anatomical MR image to an MNI template and labelling all cortical voxels according to the 78 cortical regions of interest (Gong et al., 2009). Subsequently, an inverse registration to anatomical subject space was performed and the centroid voxel for every region of interest was extracted to serve as representative voxel for every region (Hillebrand et al., 2016). Pre-computed single-shell source models are provided by the HCP at multiple resolutions (Nolte, 2003), registered into the standard co-ordinate space of the Montreal Neuroimaging Institute. Data were beamformed with depth normalisation onto centroid voxels using normalised lead fields and estimates of the data covariance. Covariance was computed within frequency specific bands (see below) with a time window spanning the whole experiment (Brookes et al., 2008). This resulted in a separate timecourse for every frequency band. Regularisation was applied to the data covariance matrix using the Tikhonov method with a regularisation parameter equal to 5% of the maximum eigenvalue of the unregularised covariance matrix. Dipole orientation was determined using a non-linear search for optimum signal to noise ratio (Robinson, 1999). This complete process resulted in 78 electrophysiological timecourses, each representative of a separate AAL region.

2.3. MEG: estimating functional networks

Functional connectivity was estimated in the context of static connectivity. For static connectivity we employed the amplitude envelope correlation metric (Brookes et al., 2011; Hipp et al., 2012). Beamformed data was frequency filtered into five frequency bands: delta (1–4 Hz), theta (4–8 Hz), alpha (8–13 Hz), beta (13–30 Hz), gamma1 (30–48 Hz) and gamma2 (48–70 Hz). This was followed by a symmetric orthogonalisation to reduce for signal leakage (Colclough et al., 2015). The Hilbert envelope was subsequently extracted from these leakage-reduced frequency-filtered timecourses followed by a computation of the Pearson's correlation between envelopes. Functional connectivity was computed within a window spanning the whole experiment and estimated between all possible pairs of timecourses forming a functional connectivity matrix. Functional connectivity matrices were subsequently averaged across subjects, resulting in one group averaged functional connectivity matrix for every frequency band.

2.4. Diffusion MRI: data acquisition and pre-processing

Diffusion MRI data were obtained from the Human Connectome Project (Van Essen et al., 2013). Full acquisition protocol details are described in (Sotiropoulos et al., 2013). Briefly, a monopolar Stejskal-Tanner echo planar imaging sequence was used in a 3T Siemens Connectom Skyra to acquire data at $(1.25\,\text{mm})^3$ isotropic resolution. Diffusion-sensitization was applied with 3 b values ($b = 1000$, 2000 and 3000 s/mm^2) and along 90 directions per b-shell. Two repeats were obtained with blip-reversed phase encoding. The minimally processed data were used (Glasser et al., 2013), where susceptibility-induced distortions, eddy currents and subject motion were all corrected simultaneously using a non-parametric framework (Andersson and Sotiropoulos, 2016) based on Gaussian processes (Andersson and Sotiropoulos, 2015).

2.5. Diffusion MRI: estimation of structural connectomes

Fibre orientations were estimated from the distortion-corrected data using a model-based deconvolution framework (Jbabdi et al., 2012; Sotiropoulos et al., 2016), implemented on GPUs (Hernández et al.,

2013) and available through FSL's bedpostx (model = 3) (Hernández et al., 2013). Up to three fibre orientations and their uncertainty were estimated per voxel using a Bayesian framework and a shrinkage prior on the volume fractions. These estimates were subsequently used for probabilistic tractography in FSL to estimate a connectome. For each subject, the white/grey matter boundary surface was used as a seed, since this reduces biases observed using whole-brain seeding (Donahue et al., 2016; Smith et al., 2015). Streamlines were seeded from 60,000 standard-space vertices (Glasser et al., 2013) on the boundary surface (10,000 streamlines per seed). Anatomical constraints were imposed to reduce false positives (Glasser et al., 2013). Specifically, we allowed streamlines to hit the white matter/grey matter boundary not more than twice, and also streamlines were allowed to enter subcortical volumes, propagate within them, but terminate upon exit. The pial surface was further used as a termination mask to ensure estimated paths do not "jump" between neighbouring gyri. The number of streamlines reaching each vertex in the WM/GM boundary was recorded, and this was normalised by the total number of valid streamlines propagated, giving a dense $60{,}000 \times 60{,}000$ structural "connectivity" matrix. Ten subjects were processed and their resulting dense connectomes were averaged. Using the AAL cortical parcellation, this average matrix was reduced to a 78×78 parcellated structural connectome, by computing for each pair of regions the mean structural connectivity between all pairs of vertices they were comprised of. The eigenmodes are then extracted by a standard eigenvalue decomposition ($W = V\Lambda V^T$), where the columns in V correspond to the eigenvectors and the diagonal elements in Λ to the eigenvalues). An eigenmode corresponds to an eigenvector and its corresponding eigenvalue. Note that the eigenmodes can be considered as basis set for the structural connectome or considered as patterns embedded in the structural connectome. Fig. S1 shows how a range of thresholds for the structural connectome affects the eigenmodes.

2.6. Linear stability analysis of a network of neural mass models

If structural eigenmodes can indeed be regarded as a basis set for MEG networks, we anticipate that an additional step is required to translate these eigenmodes into function. More specifically, we hypothesize that we require dynamics to excite or activate structural sub-networks described by the eigenmodes in the right proportion in order to be expressed at the functional network level. To test this hypothesis, we consider a network of neural mass models, each representing a grey matter region as defined by the AAL atlas and all coupled together using an AAL-parcellated structural connectome. We linearise the neural mass model around the steady state, so that we can analytically predict the eigenmodes that can be excited or activated, even in the presence of conduction delays.

We refer to the supplementary material for a full derivation of the linearised networks. Let us first consider a single neural mass model, whose dynamics are described by a state vector $\boldsymbol{x}(t) = (\mathbf{x}^1(t),\ldots,\mathbf{x}^m(t))$, where m corresponds to the dimension of the chosen model. For example, the Jansen-Rit model (Jansen and Rit, 1995) has 6 dimensions, whereas the Wilson-Cowan model (Wilson and Cowan, 1972) only has 2. For the moment, we ignore delays and we consider a network of N neural masses, with identical neural masses placed on each node of the network

$$\frac{dx_i}{dt} = F(x_i) + G\left(w^{loc}x_i + s_i\right) \tag{1}$$

where $i = 1,\ldots,N$. Here, F describes the intrinsic dynamics of the node in the absence of coupling, and G the dynamics induced by synaptic coupling, from both local and network mediated interactions. The local (within node) connections are described by the matrix w^{loc} and s represents the input from other nodes in the network,

$$s_i = \eta \sum_{j=1}^{N} w_{ij} H\left(x_j\right) \tag{2}$$

where H corresponds to the local component of the node which mediates the interactions between nodes, through the structural connectivity matrix W (with components w_{ij}) with coupling strength η. Remember that x_i is itself a vector ($x_i(t) \in \mathbb{R}^m$). For the moment, we suppress a discussion of time-delays, though will return to this shortly.

Let us assume that there exists a steady state $\bar{x}_i = (\bar{x}_i^1,\ldots,\bar{x}_i^m)$, where $(F(\bar{x}_i) + G(w^{loc}\bar{x}_i + \bar{s}_i) = 0)$ with $\bar{s}_i = \sum_{j=1}^{N} w_{ij}H(\bar{x}_j)$. We apply a small perturbation of the form $x_i(t) = \bar{x}_i + u_i(t)$ to obtain the following linearised system,

$$\frac{du_i}{dt} = \left[DF(\bar{x}_i) + DG\left(w^{loc}\bar{x}_i + \bar{s}_i\right)w^{loc}\right]u_i + \sum_{j=1}^{N} DG\left(w^{loc}\bar{x}_i + \bar{s}_i\right)DH\left(\bar{x}_j\right)w_{ij}u_j \tag{3}$$

where $DF, DG, DH \in \mathbb{R}^{mxm}$ are Jacobians. These equations can be block diagonalised to obtain a decoupled set of equations for determining linear stability, indexed by the eigenvalues of the structural connectivity matrix W. These in turn specify the eigenvalues of the linearised network dynamics according to the following spectral equation (see supplementary material for a full derivation)

$$\varepsilon(\lambda;p) = \det\left[\lambda I_m - D\tilde{F}_p - \mu_p D\tilde{G}_p\right] = 0 \;\; with \;\; p = 1,\ldots,N \tag{4}$$

Here, we have introduced the abbreviations $D\tilde{F}_i = DF(\bar{x}_i) + DG(w^{loc}\bar{x}_i + \bar{s}_i)w^{loc}$ and $D\tilde{G}_i = DG(w^{loc}\bar{x}_i + \bar{s}_i)DH(\bar{x}_j)$. Furthermore, I_m refers to an $m \times m$ identity matrix, λ corresponds to the eigenvalues of the system (linearised network; equation (3)), while μ_p corresponds to the eigenvalue corresponding to the *p-th* eigenvector of the structural network W. The last expression enables us to analyse the stability of the system in terms of the eigenvectors of the structural network W. This general form can be applied to any network of neural masses.

If we now consider a network of Wilson-Cowan models

$$\frac{d}{dt}\begin{bmatrix}\tau_E E_i \\ \tau_I I_i\end{bmatrix} = -\begin{bmatrix}E_i \\ I_i\end{bmatrix} + f\begin{pmatrix} w^{EE}E_i + w^{EI}I_i + P + \sum_{j=1}^{N} w_{ij}E_j \\ w^{IE}E_i + w^{II}I_i \end{pmatrix} \tag{5}$$

where E and I refer to the firing rates of excitatory and inhibitory populations, τ_a to the time constant determining the magnitude of the exponential decay, P an external input and $f = [f_E\, f_I]^T$, where f_a is a sigmoid function obeying $f_a = 1/(1 + \exp(\beta(x - \theta_a)))$, with $a \in \{E, I\}$. We can now determine $D\tilde{F}_p$ and $D\tilde{G}_p$ for the Wilson-Cowan model

$$D\tilde{F}_p = -\begin{bmatrix}\tau_E & 0 \\ 0 & \tau_I\end{bmatrix}^{-1}\left[I_2 - Df\left(w^{loc}\bar{x}_i + \bar{s}_i\right)\right]w^{loc}$$

$$D\tilde{G}_p = \begin{bmatrix}\tau_E & 0 \\ 0 & \tau_I\end{bmatrix}^{-1}\left[I_2 - Df\left(w^{loc}\bar{x}_i + \bar{s}_i\right)\right]\begin{bmatrix}1 & 0 \\ 0 & 0\end{bmatrix} \tag{6}$$

This allows us to rewrite the spectral equation (4) as

$$\varepsilon(\lambda;p) = \det\left[\lambda I_2 + \begin{bmatrix}\tau_E & 0 \\ 0 & \tau_I\end{bmatrix}\left\{I_2 - Df\left(w^{loc}\bar{x}_p + \bar{s}_p\right)\left[w^{loc} + \begin{bmatrix}\mu_p & 0 \\ 0 & 0\end{bmatrix}\right]\right\}\right] = 0 \tag{7}$$

In the presence of axonal conduction delays, $s_i(t) = \eta\sum_{j=1}^{N} w_{ij}H(x_j(t - \tau_{ij}))$, and μ_p now takes the form

$$\mu_p(\lambda) = \sum_{i=1}^{N}\sum_{i=1}^{N} w_{ij}\exp\left(-\lambda\tau_{ij}\right)v_i^p v_j^p \tag{8}$$

where τ_{ij} refers to the conduction delay between node i and j in the

network and v_j^p to the *j-th* element in the *pth* eigenvector of the structural network. This makes the spectral equations (4) and (7) transcendental functions, which can only be solved numerically. A solution to the spectral equations (4) and (7) is stable if $Re(\lambda) < 0$. A bifurcation occurs when an eigenvalue crossed through the imaginary axis $Re(\lambda) = 0$. Two types of instability can occur: 1) when a real eigenvalue crosses from the left hand complex plane to the right ($Im(\lambda) = 0$) (static bifurcation, i.e. a transition between fixed points) or when a complex conjugate pair of eigenvalues cross from the left hand complex plane to the right ($Im(\lambda) \neq 0$) (dynamic bifurcation, i.e. a transition between a fixed point and limit cycles). The value of p for which bifurcation occurs allows us to determine which pattern of network activity will be excited. More specifically, we refer to 'eigenmode-excitation' as being associated to an instability of a network steady state, with the emergent network pattern associated to the first eigenvalue to cross the imaginary axis. This complex eigenvalue, from linear stability analysis, is itself parameterised by a real eigenvalue of the (symmetric) structural connectivity matrix, and thus can be used to determine the spatial pattern of excitation. Note that linear stability only holds in the vicinity of the bifurcation.

2.7. Analysis steps

1. We address whether we can we predict frequency band specific MEG networks using the eigenvectors of the structural connectome. This is done in two steps. *First*, we predict whether the functional connectivity matrix A_f (f = frequency band), can be explained in terms of a linear combination of the eigenvectors of the structural network: $\tilde{A}_f = \sum_{p=1}^{N} c_{pf} v^p (v^p)^T$, where c_{pf} are constants that are estimated using a non-linear least squares fitting method. To assess whether this prediction could be obtained by chance or any random set of similarly structured eigenvectors we compared the resulting R^2 from the prediction based on real data with a null distribution (10,000 realisations). The null distribution of R^2 is obtained by fitting pseudo-eigenmodes to MEG connectivity matrices. Construction of the pseudo-eigenmodes is described in (Tewarie et al., 2016a) and recently applied in (Hunt et al., 2016). Briefly, the eigenvectors are treated as timeseries and Fourier transformed. A random number is added to the phases in Fourier domain, followed by an inverse Fourier transformation to construct a pseudo-eigenvector. This method ensures that the pseudo-eigenvectors have the same smoothness as the original eigenvectors. *Second*, we analyse the number of eigenvectors that significantly contribute to the prediction. We sequentially predict the frequency specific functional connectivity matrices using the eigenvectors of the structural network in sequential steps, i.e. first adding the first eigenvector to the prediction, then the second and so on. We keep track whether the increase in R^2 is larger than an increase in R^2 based on pseudo-vectors after adding a new eigenvector to the prediction. Only the eigenvectors of the structural network that outperform the pseudo-eigenvectors are kept for the eventual prediction. This will eventually result in a set of eigenvectors of the structural network required for the prediction.
2. We address whether we can excite the relevant set of eigenvectors of the structural network (see previous point) using linear stability analysis of Wilson-Cowan networks. We first numerically solve the spectral equation (7) in the absence of delays as a function of P (external input or drive to all populations) for all eigenvectors of the structural network. We then include equation (8) and solve equation (7) with delays. The delays are based on the Euclidean distances d_{ij} between regions in the AAL atlas divided by a conduction velocity v (10 m/s assumed in this paper (Deco et al., 2009)) plus an additional offset delay τ_0, i.e. $\tau_{ij} = \frac{d_{ij}}{v} + \tau_0$. The offset delay can be interpreted as the time to synchronise in individual neuronal populations. An offset delay has been shown to lead to dynamics reminiscent of those seen in simulations of large-scale spiking networks (Roxin et al., 2005), and its physiological interpretation can be connected to the relaxation time-scale for which spiking networks can reasonably allow for a firing rate description.
3. The parameter settings for P and τ_0 as obtained from linear stability analysis for which the correct set of eigenmodes are excited (see analysis step 1) are fed into the simulations. We simulate a network of Wilson-Cowan oscillators using the same structural network as in the previous steps. We turn to simulations for two reasons: 1) to verify the results obtained from the previous section and 2) to analyse the regime further away from the bifurcation, where linear stability theory loses its validity. In this regime eigenmodes can interact in a nonlinear fashion which cannot be tracked using linear stability analysis. We numerically solve equation (5) in the presence of delays using a Heun integration scheme. The Heun scheme was implemented to induce fluctuations for the steady state regime. The last term in the first row of equation (5) becomes $\sum_{j=1}^{N} w_{ij} E_j \left(t - \frac{d_{ij}}{v} + \tau_0 \right)$. The amplitude envelope correlation is subsequently computed between all possible region pairs forming a functional connectivity matrix. This matrix is then used for a prediction of empirically observed functional connectivity matrices, resulting in an R^2 for every prediction. Parameters for the Wilson-Cowan network simulations were the same as in (Abeysuriya et al., 2018).

3. Results

3.1. Estimating frequency band specific networks based on structural eigenmodes

Fig. 1AB illustrates the structural connectome in terms of its weighted adjacency matrix and the variance of the structural connectome explained by the first n eigenmodes. For illustrational purposes, the first six eigenmodes of the structural network are projected to a brain to demonstrate the clear structure or patterns in these eigenmodes, such as a sensorimotor pattern, an occipital pattern, a frontal pattern or a pattern with dominant regions in the cingulate areas (Fig. 1C). The group averaged functional connectivity matrices for the different frequency bands obtained from MEG data are shown in Fig. 2A. The four blocks in the alpha band correspond to connections between posterior regions. These are also present in the theta, gamma1 and beta band. In addition, the beta, gamma1 and theta band connectivity matrices contain additional connectivity patterns, such as sensorimotor and frontal connections. We then predicted these frequency band specific functional connectivity matrices using a linear combination of all the eigenmodes of the structural network ($\tilde{A}_f = \sum_{p=1}^{N} c_{pf} v^p (v^p)^T$), which is depicted in Fig. 2B. The functional connections projected onto a brain show a clear frontal pattern of connections in estimation of the delta and gamma2 band networks, frontal and posterior connections in the theta band, posterior connections in the alpha band, posterior, sensorimotor and frontal connections in the beta band and a diffuse pattern of connectivity in the gamma bands. The best estimation for functional networks based on the eigenmodes was obtained for the alpha band network (see R^2 in Fig. 2E). To analyse whether the estimation of the functional connectivity matrices from the eigenmodes of the structural network could be obtained by chance, we repeated the prediction from the eigenmodes to function with pseudo-eigenmodes of the structural connectome (surrogate data). Results show clearly that the prediction with the real structural connectivity matrices outperform the prediction with surrogate data (Fig. S2), suggesting that the eigenmodes from the structural network may form a genuine basis for the empirical functional networks. Lastly, we analysed whether an increase in R^2 after addition of individual eigenmodes to the prediction of the MEG networks could outperform the addition of a pseudo eigenmode. Results show that only the first 6 eigenmodes were contributing significantly to the prediction of the frequency band specific

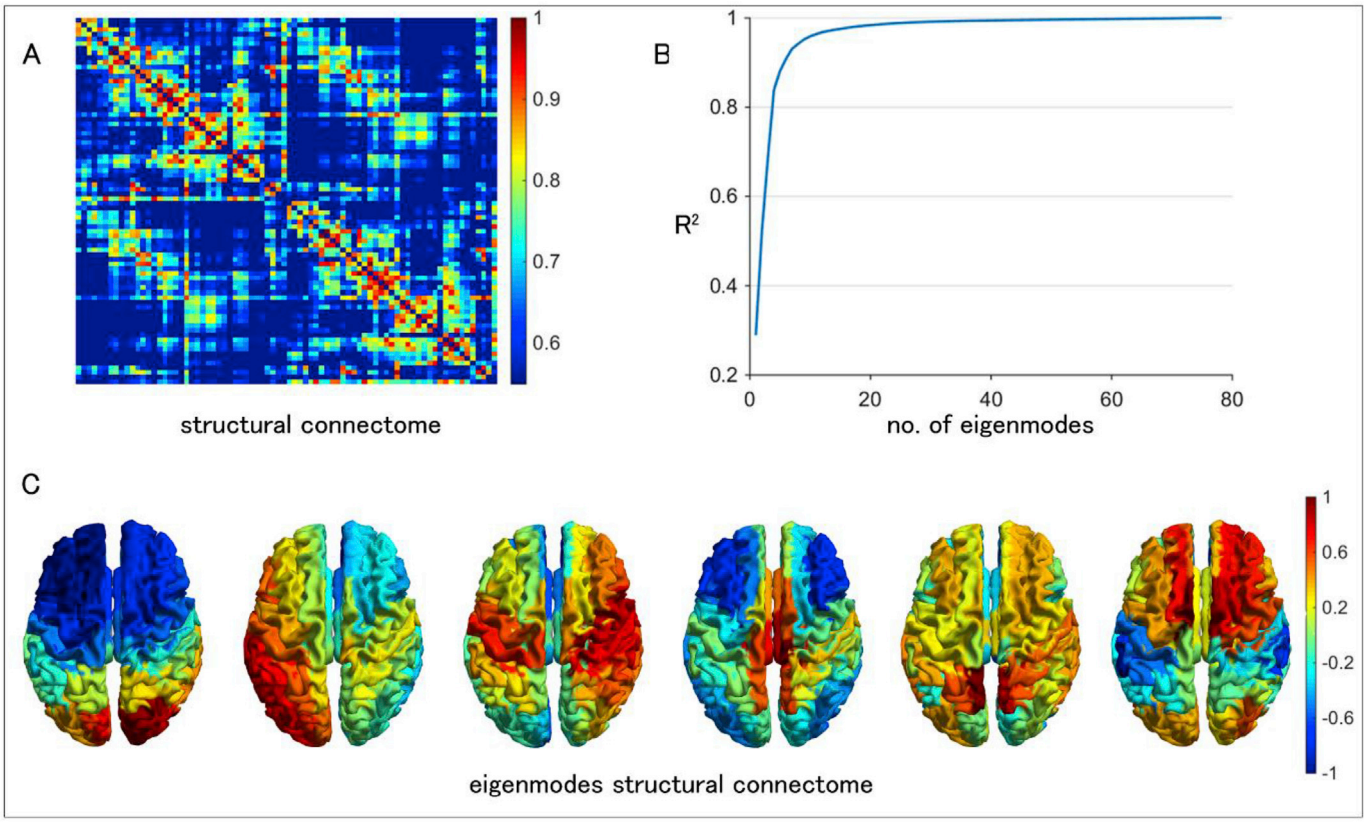

Fig. 1. Structural connectome: (A) The weighted adjacency matrix of the structural connectome with a link density of 0.37. (B) The variance of structural connectome (R^2) explained by the first n structural eigenmodes. The variance explained for n number of eigenmodes in the graph corresponds to the set from the first eigenmode on to the nth eigenmode. (C) As an illustration, the first six eigenvectors of the structural connectome are depicted from left to right in an ascending order.

MEG networks. Results are shown in Fig. S3 and in Fig. 2D. The latter shows the estimated coefficients for the first six eigenmodes in the eigenmode prediction of the empirical frequency specific connectivity matrices.

3.2. Linear stability analysis of a network of neural mass models

The previous analysis suggests that frequency band specific networks can to some extent be represented using the eigenmodes of the structural network. In this section, we demonstrate how the right set of eigenmodes can be excited using linear stability analysis of the time independent steady state of a network of neural masses. We remind the reader that bifurcation occurs when an eigenvalue (λ) of the system defined by equation (4) crosses the imaginary axis $Re(\lambda) = 0$. As mentioned in the Methods section, equations (4) and (7) allow us to analyse the stability of the system in terms of μ_i.

We first chose to ignore delays and tune the external drive to the individual nodes P, to determine where bifurcation occurs. We found that bifurcation occurs at $P = 0.26$ (Fig. 3A and B), and as P is increased further more eigenmodes become unstable (Fig. 3B). Note that the 1st eigenmode is always the one to go unstable at the bifurcation (Fig. 3A). Analysis was carried out for several runs of the same numerical analysis (hence the rate of occurence in Fig. 3A). As the structural connectivity matrix W is symmetric, the eigenvalues are all real and we can order them such that $\mu_1 > \mu_2 > \ldots > \mu_N$. When solving equation (7) in the case of no delays, this ordering of the eigenmodes will be reflected in the ordering of the eigenvalues of the system. Fig. 3C shows the eigenspectrum of the system close to the bifurcation in the case for no delays (solution to equation (7)). Fig. 3D shows the eigenspectrum as P is increased past the bifurcation point. A bifurcation occurs when the eigenvalues cross the imaginary axis from the left. The unstable eigenvalues are highlighted in red, it is clear to see that there are a number of unstable eigenvalues for this choice of P ($P = 0.28$). It is important to note that linear stability analysis only holds provided we are sufficiently close to the bifurcation point.

If we now include delays plus an additional delay offset (τ_0), eigenmodes other than the first eigenmode can lose their stability at the bifurcation (Fig. 4A). In other words, inclusion of delays allows for reordering of the eigenmodes that can be excited first. The expression of these various other eigenmodes also allows for a richer repertoire of connectivity patterns at the functional level. Fig. 4B is the equivalent of Fig. 3B, but now in the presence of delays and shows the number of unstable of eigenmodes when both P and τ_0 are tuned (the non-smoothness in Fig. 4B is due to discretness). A bifurcation occurs when the real part of the system eigenvalues cross the imaginary axis, from left to right, in the complex plane. Fig. 4C shows an example of the eigenspectrum just after the bifurcation for a small offset delay. Here again the first eigenmode is the first one that crosses the imaginary axis from the left and thus loses stability at the bifurcation (complex conjugate pair in this case). However, other choices for offset delays allow to excite other eigenmodes and furthermore allow to excite eigenmodes nearly simultaneously (see Fig. 4D–H). If delays cause the simultaneous excitation of two modes, then the resulting temporal pattern will mix their frequencies. Fig. 4E is an example that shows the correct set of eigenmodes obtained in the previous section to explain empirical MEG networks.

3.3. Predicting frequency band specific networks from a simulated network of neural mass models

In the last section we have demonstrated that the correct set of eigenmodes can be excited in the presence of delays using linear stability analysis. We now turn to simulations to verify the results obtained by

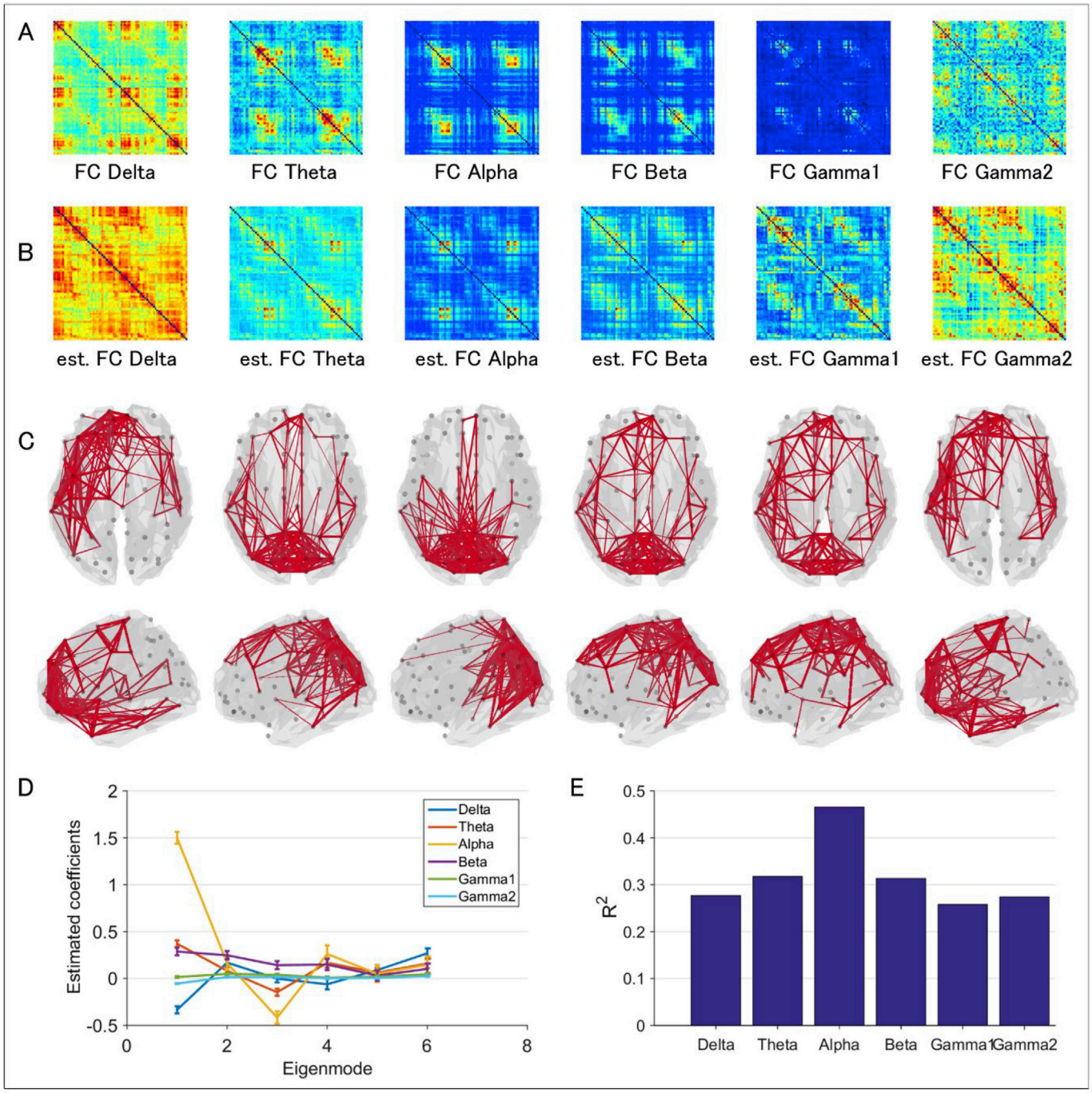

Fig. 2. Prediction of frequency band specific networks based on the eigenmodes: (A) Frequency band specific functional connectivity matrices based on AEC and MEG data. (B) Predicted functional connectivity matrices based on a linear weighted sum of the first six eigenmodes of the structural connectome. Colours in A and B correspond to connectivity strength (C) Predicted functional connections using a linear weighted sum of the structural eigenmodes, illustrated in glass brain plots. (D) shows the estimated coeffiicients for the first six eigenmodes, i.e. it shows how much each eigenmode contributes to a frequency band specific prediction. Error bars correspond to the confidence intervals of the estimated coefficients. (E) shows how much of the variance (R^2) of the empirical functional connectivity matrices can be explained by a linear combination of the eigenmodes for each frequency band separately.

linear stability analysis and also analyse the regime further away from the bifurcation, i.e. further away from the stable regime. We would like to remind the reader that by definition, the bifurcation separates the steady state from an oscillatory regime. Furthermore, linear stability analysis does not predict in which proportion the eigenmodes will be excited or how they interact once the bifurcation is crossed. We simulate equation (5) with the offset delay from the previous section (Fig. 4E) and vary P with an initial value before the bifurcation and a final value well after the bifurcation. Fig. 5A shows the goodness of fit (R^2) of the model output with empirical MEG functional networks for the different frequency bands. The best fit for the alpha and theta band networks was after the bifurcation ($P = 0.28$), while the beta band network has the optimal fit even further away from the bifurcation. The delta (dark blue curve), gamma1 (green curve) and gamma2 band (light blue curve) networks are consistent with simulations well after the bifurcation. The best fits of the model in the presence of delays for the different frequency bands (i.e. maxima of Fig. 5A) are illustrated in Fig. 5D. Fig. 5B shows the goodness of fit for different values of P in the absence of delays. It can be observed

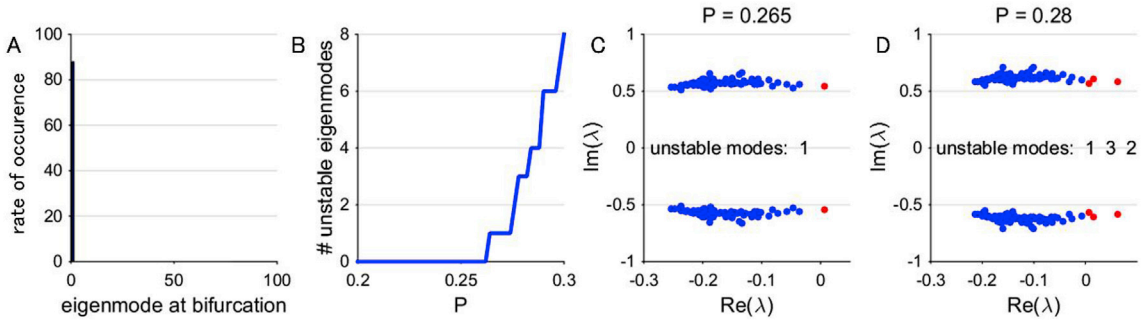

Fig. 3. Linear stability analysis of a network of neural mass models in the absence of delays: (A) the eigenmodes that become unstable at the bifurcation. It is always the first eigenmode in the absence of delays that crosses the bifurcation and thus loses stability. This bifurcation occurs for P = 0.26 (B), i.e. this is the value for P when an eigenmode loses stability. By increasing P further, other eigenmodes also lose their stability (B). (E) shows the eigenspectrum of the system right after the bifurcation in the absence of delays. Here only the first eigenmode loses stability (complex conjugate pair) (F) shows an example of the spectrum in the absence of delays further away from the bifurcation when multiple eigenmodes lose their stability. Blue dots in (C-D) correspond to λ that are stable, while red dots correspond to λ that are unstable and thus excited.

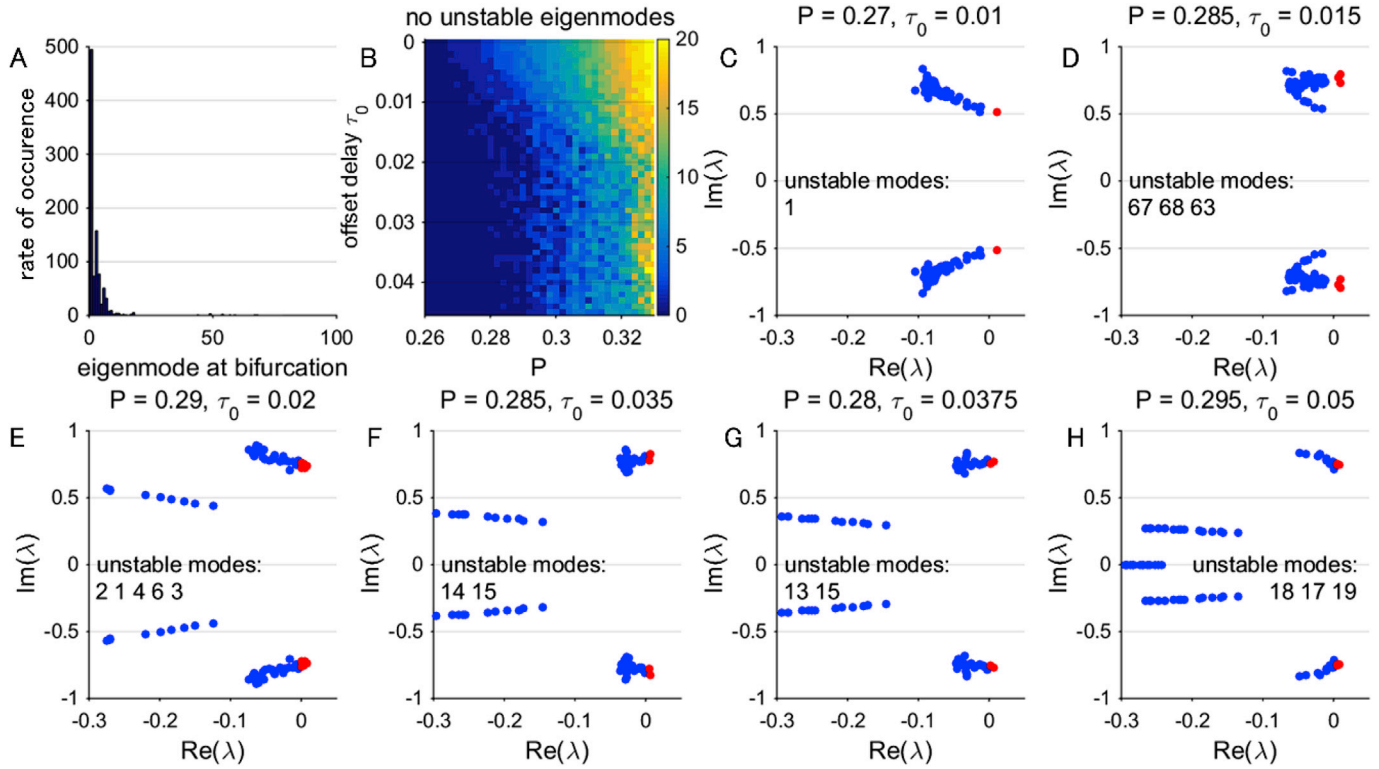

Fig. 4. Linear stability analysis of a network of neural mass models in the presence of delays: (A) the eigenmodes that lose their stability at the bifurcation. Delays allow other eigenmodes than the first one to lose their stability at the bifurcation. A bifurcation occurs in (B) when the real part of the system eigenvalues cross the imaginary axis in the complex plane. Both P and τ_0 are tuned in (B). (C-F) show different eigenspectra for different values for the offset delay (τ_0), and demonstrate how various other eigenmodes can be excited at the bifurcation. It also demonstrates how the presence of delays allows to excite eigenmodes nearly simultaneously. (E) shows the eigenspectra where the correct eigenmodes (Fig. 2D) are excited nearly simultaneously. Blue dots in (C-H) correspond to λ that are stable, while red dots correspond to λ that are unstable and thus excited.

that the goodness of fit values are lower than for the simulations with delays. This seems to be related to the observation that with simulations with no delays, the first eigenmode is most of the time strongly dominating the emergent functional connectivity pattern. Fig. 5C shows the correlation of the simulated functional connectivity matrix with the first eigenmode of the structural connectome. These correlation values in the case for no delays are stronger than the case for delays, when other eigenmodes are also expressed. From Fig. 4, we can see that the complex part of subsequent crossing eigenvalues are very similar, hence the mixing of frequencies will happen in a restricted range. This can be seen in Fig. S4, which shows the power spectra presented from the simulations in Fig. 5 and shows peak broadening with subsequent eigenmode excitations.

4. Discussion

We aimed to explain how different frequency specific MEG networks emerge from one underlying structural network. Our results show that different frequency band specific MEG networks can be predicted by a set of eigenmodes of the structural network. We demonstrated using linear stability analysis that we require the inclusion of conduction delays in a system of neural masses to excite the correct set of eigenmodes in order to

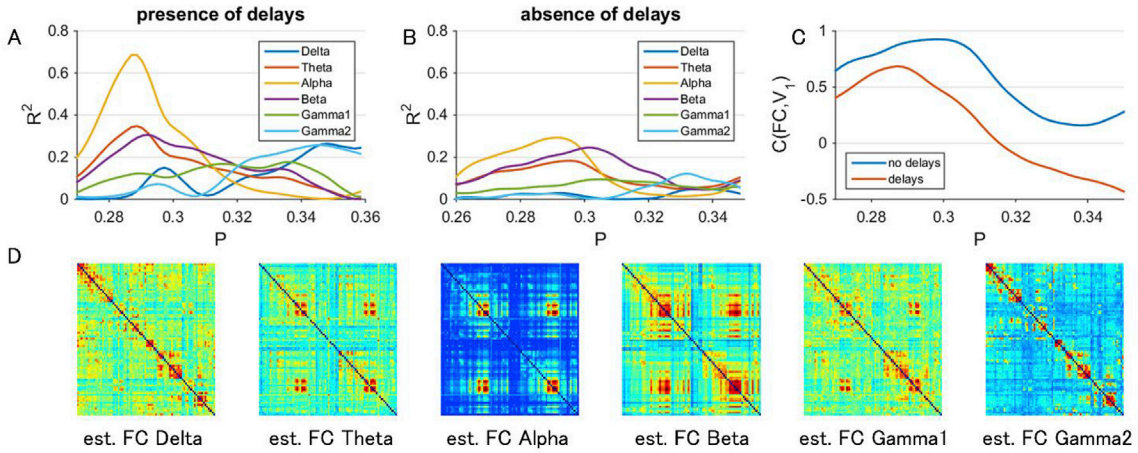

Fig. 5. Simulations of a network of neural masses in the presence and absence of delays: (A) shows the goodness of fit in terms of the R^2 between simulated functional connectivity matrices and MEG connectivity matrices for different values for P, for different frequency bands in the presence of delays. (B) shows the equivalent of (A) in the absence of delays. (C) shows the correlation between simulated functional connectivity matrices and the first eigenmode of the structural connectome in the absence (blue) and presence (red) of delays for various values for P. (D) shows the best fits for the model output with empirical MEG data. The matrices correspond to values for P for which the curves in (A) are maximal.

be consistent with the empirical MEG data. Simulations with the Wilson-Cowan model showed that near the bifurcation where the modes become unstable, functional connectivity patterns emerge that are most consistent with the alpha, theta and beta MEG networks, while the gamma and delta bands are consistent with simulated networks well after the bifurcation.

We predicted frequency specific MEG networks using a linear combination of the eigenmodes of the structural network. Statistical testing with surrogate data showed that these predictions could not be obtained by chance, emphasizing the genuine plausibility of these predictions. A crucial aspect with respect to the discussion is the interpretation of the eigenmodes in the context of neurophysiology. Apart from the fact that they form a basis set for the structural network, they can also be regarded as a set of patterns of activity. If we regard the structural network as a transformation of this pattern of activity, then only the magnitude of the activities change, but not the pattern. Thus, we could also interpret these structural eigenmodes as dominant patterns that are supported by the structural network. Previous work on eigenmodes has mostly focused on fMRI networks, where predictions from both the eigenmodes of the cortical surface (Robinson et al., 2016) as well as the eigenmodes of the structural network (Atasoy et al., 2016) were consistent with resting state fMRI networks. In our previous paper on MEG networks, we decomposed the connectivity matrices of the functional networks in terms of eigenmodes of function and demonstrated that frequency band specific networks were characterised by a common mode superimposed by a frequency band specific mode (Tewarie et al., 2016b). The current work approaches this topic from a different angle by analysing a structure-function relationship instead. Despite this different angle, the current findings could explain that this previously found common mode might be a product of excitation of the eigenmodes of the structural network. Lastly, only a limited set of eigenmodes contributed significantly to the prediction of the MEG networks (eigenmodes 1–6). However, it cannot be excluded that the limited set could be due to inaccuracies in the estimation of structural connections (tractography pipeline) or due to inaccuracies in the estimation of functional connections (Sotiropoulos and Zalesky, 2017).

Despite surviving statistical testing, the statistical prediction of frequency specific MEG network based on the eigenmodes of the structural network does not explain how the eigenmodes are translated into function or functional networks. In order to understand how these eigenmodes are translated into MEG networks we show using linear stability analysis how these eigenmodes become unstable in a network of neural masses and hence how they project to functional networks. In order to excite the relevant set of eigenmodes the system requires the inclusion of conduction delays. Without delays, it is hard to see how the real part of the eigenvalues can cross the imaginary axis simultaneously or in a different order. Note, however that this is not the first computational neuroscience analysis that supports the notion of delays in a network of neural masses to be consistent with empirical networks. A crucial role for the inclusion of delays has also been stressed in the context of temporally evolving networks (Deco et al., 2009; Cabral et al., 2017; O'Neill et al., 2017). Previous studies also stressed the importance of delays between network nodes in shaping frequency specific MEG networks (Cabral et al., 2014; Abeysuriya et al., 2018). However, to our knowledge, this is the first time that the importance of offset delays in relation to eigenmode excitation is stressed in the context of frequency specific MEG networks. Frequency specific networks could be explained near a working point of the network of neural masses around the bifurcation (for alpha, beta and theta), and further away from the bifurcation for the delta, gamma1 and gamma2 networks. It remains to be elucidated whether the generators for neuronal oscillations in the different frequency bands might correspond to different working points from a bifurcation.

A few points with respect to the methodology and findings deserves to be mentioned. A limitation from the current linear stability analysis is that the complex part of the system eigenvalues for a given eigenmode does not correspond one to one with the MEG frequency bands (see Fig. 4C–H). In recent work we demonstrate how this could be improved by analysing beyond fixed point instabilities. We show how to construct periodic (synchronous) network oscillations and determine their stability (Coombes et al., 2018). Future work will need to extend this into other phase-locked states and demonstrate a better match with the natural occurring frequencies in empirical data. Secondly, the nodes in the Wilson Cowan network all had identical dynamics, future work could incorporate a heterogenous network of Wilson Cowan nodes as a further more realistic extension, or the use of next generation neural mass models (Byrne et al., 2017; Coombes and Byrne, 2019). Thirdly, an alternative explanation for the emergence of frequency band specific networks is that their spatial structure is merely the result of spatial topography of signal to noise (SNR) ratio across the brain. However, our previous study suggests that modulations in amplitude envelopes themselves (thus fluctuations in SNR) might be a consequence of long range connectivity (Tewarie et al., 2018). Fourthly, we used Euclidean distances to estimate interregional conduction delays (Abeysuriya et al., 2018; Cabral et al., 2014; Ghosh et al., 2008; Hellyer et al., 2015; Tewarie et al., 2016b) rather than curved streamline distance, which would be the

more realistic case. Fifthly, there is no unique classification of the MEG frequency bands, although we used a quite common classification also used by several other groups (Coquelet et al., 2017; Demuru et al., 2017; Engels et al., 2017; López et al., 2017; Ranasinghe et al., 2017; Seymour et al., 2018). Lastly, our analysis were limited by the fact that we merely employed amplitude envelope correlation as connectivity metric. However, note that amplitude envelope correlation and phase based metric show high correlation in predominantly resting state connectivity data (Colclough et al., 2016; Tewarie et al., 2014).

In summary, we have demonstrated how frequency band specific networks can emerge in a system of neural masses with conduction delays, where different frequency band specific networks were shown to emerge at slightly different working points of the system. For different working points away from the bifurcation a selected set of structural eigenmodes can become excited to coherently emerge as frequency specific network structure.

Acknowledgments

This work was funded by a Medical Research Council New Investigator Research Grant (MR/M006301/1) awarded to MJB. We also acknowledge Medical Research Council Partnership Grant (MR/K005464/1).

Supplementary data

Supplementary data to this article can be found online at https://doi.org/10.1016/j.neuroimage.2018.10.079.

References

Abeysuriya, R.G., Hadida, J., Sotiropoulos, S.N., Jbabdi, S., Becker, R., Hunt, B.A.E., Brookes, M.J., Woolrich, M.W., 2018. A biophysical model of dynamic balancing of excitation and inhibition in fast oscillatory large-scale networks. PLoS Comput. Biol. 14 e1006007.

Alexander-Bloch, A.F., Vértes, P.E., Stidd, R., Lalonde, F., Clasen, L., Rapoport, J., Giedd, J., Bullmore, E.T., Gogtay, N., 2012. The anatomical distance of functional connections predicts brain network topology in health and schizophrenia. Cereb. cortex 23, 127–138.

Amico, E., Marinazzo, D., Di Perri, C., Heine, L., Annen, J., Martial, C., Dzemidzic, M., Kirsch, M., Bonhomme, V., Laureys, S., 2017. Mapping the functional connectome traits of levels of consciousness. Neuroimage 148, 201–211.

Andersson, J.L.R., Sotiropoulos, S.N., 2015. Non-parametric representation and prediction of single-and multi-shell diffusion-weighted MRI data using Gaussian processes. Neuroimage 122, 166–176.

Andersson, J.L.R., Sotiropoulos, S.N., 2016. An integrated approach to correction for off-resonance effects and subject movement in diffusion MR imaging. Neuroimage 125, 1063–1078.

Ashwin, P., Coombes, S., Nicks, R., 2016. Mathematical frameworks for oscillatory network dynamics in neuroscience. J. Math. Neurosci. 6, 2.

Atasoy, S., Donnelly, I., Pearson, J., 2016. Human brain networks function in connectome-specific harmonic waves. Nat. Commun. 7.

Bassett, D.S., Sporns, O., 2017. Network neuroscience. Nat. Neurosci. 20, 353.

Bassett, D.S., Wymbs, N.F., Porter, M.A., Mucha, P.J., Carlson, J.M., Grafton, S.T., 2011. Dynamic reconfiguration of human brain networks during learning. Proc. Natl. Acad. Sci. Unit. States Am. 108, 7641–7646.

Bettinardi, R.G., Deco, G., Karlaftis, V.M., Van Hartevelt, T.J., Fernandes, H.M., Kourtzi, Z., Kringelbach, M.L., Zamora-López, G., 2017. How structure sculpts function: unveiling the contribution of anatomical connectivity to the brain's spontaneous correlation structure. Chaos An Interdiscip. J. Nonlinear Sci. 27, 47409.

Brookes, M.J., Vrba, J., Robinson, S.E., Stevenson, C.M., Peters, A.M., Barnes, G.R., Hillebrand, A., Morris, P.G., 2008. Optimising experimental design for MEG beamformer imaging. Neuroimage 39, 1788–1802.

Brookes, M.J., Hale, J.R., Zumer, J.M., Stevenson, C.M., Francis, S.T., Barnes, G.R., Owen, J.P., Morris, P.G., Nagarajan, S.S., 2011. Measuring functional connectivity using MEG: methodology and comparison with fcMRI. Neuroimage 56, 1082–1104.

Byrne, Á., Brookes, M.J., Coombes, S., 2017. A mean field model for movement induced changes in the beta rhythm. J. Comput. Neurosci. 43, 143–158.

Cabral, J., Luckhoo, H., Woolrich, M., Joensson, M., Mohseni, H., Baker, A., Kringelbach, M.L., Deco, G., 2014. Exploring mechanisms of spontaneous functional connectivity in MEG: how delayed network interactions lead to structured amplitude envelopes of band-pass filtered oscillations. Neuroimage 90, 423–435.

Cabral, J., Kringelbach, M.L., Deco, G., 2017. Functional connectivity dynamically evolves on multiple time-scales over a static structural connectome: Models and mechanisms. Neuroimage 160, 84–96.

Cavanna, F., Vilas, M.G., Palmucci, M., Tagliazucchi, E., 2017. Dynamic functional connectivity and brain metastability during altered states of consciousness. Neuroimage 180, 383–395.

Colclough, G.L., Brookes, M.J., Smith, S.M., Woolrich, M.W., 2015. A symmetric multivariate leakage correction for MEG connectomes. Neuroimage 117, 439–448.

Colclough, G.L., Woolrich, M.W., Tewarie, P.K., Brookes, M.J., Quinn, A.J., Smith, S.M., 2016. How reliable are MEG resting-state connectivity metrics? Neuroimage 138, 284–293.

Coombes, S., 2010. Large-scale neural dynamics: simple and complex. Neuroimage 52, 731–739.

Coombes, S., Byrne, Á., 2019. Next generation neural mass models. In: Torcini, A., Corinto, F. (Eds.), Nonlinear Dynamics in Computational Neuroscience. Springer.

Coombes, S., Lai, Y.M., ŞAYLI, M., Thul, R., 2018. Networks of piecewise linear neural mass models. Eur. J. Appl. Math. 1–22.

Coquelet, N., Mary, A., Peigneux, P., Goldman, S., Wens, V., De Tiège, X., 2017. The electrophysiological connectome is maintained in healthy elders: a power envelope correlation MEG study. Sci. Rep. 7, 13984.

Deco, G., Cabral, J., Woolrich, M.W., Stevner, A.B.A., van Hartevelt, J., Kringelbach, M.L., 2017. Neuroimage 152, 538–550.

Deco, G., Jirsa, V., McIntosh, A.R., Sporns, O., Kötter, R., 2009. Key role of coupling, delay, and noise in resting brain fluctuations. Proc. Natl. Acad. Sci. Unit. States Am. 106, 10302–10307.

Deco, G., McIntosh, A.R., Shen, K., Hutchison, R.M., Menon, R.S., Everling, S., Hagmann, P., Jirsa, V.K., 2014. Identification of optimal structural connectivity using functional connectivity and neural modeling. J. Neurosci. 34, 7910–7916.

Demuru, M., Gouw, A.A., Hillebrand, A., Stam, C.J., Dijk, B.W., Scheltens, P., Tijms, B.M., Konijnenberg, E., Kate, M., Braber, A., 2017. Functional and effective whole brain connectivity using magnetoencephalography to identify monozygotic twin pairs. Sci. Rep. 7, 9685.

Donahue, C.J., Sotiropoulos, S.N., Jbabdi, S., Hernandez-Fernandez, M., Behrens, T.E., Dyrby, T.B., Coalson, T., Kennedy, H., Knoblauch, K., Van Essen, D.C., 2016. Using diffusion tractography to predict cortical connection strength and distance: a quantitative comparison with tracers in the monkey. J. Neurosci. 36, 6758–6770.

Engels, M.M.A., Yu, M., Stam, C.J., Gouw, A.A., van der Flier, W.M., Scheltens, P., van Straaten, E.C.W., Hillebrand, A., 2017. Directional information flow in patients with Alzheimer's disease. A source-space resting-state MEG study. NeuroImage Clin 15, 673–681.

Gabay, N.C., Robinson, P.A., 2017. Cortical geometry as a determinant of brain activity eigenmodes: neural field analysis. Phys. Rev. E 96, 32413.

Garcés, P., Pereda, E., Hernández-Tamames, J.A., Del-Pozo, F., Maestú, F., Ángel Pineda-Pardo, J., 2016. Multimodal description of whole brain connectivity: a comparison of resting state MEG, fMRI, and DWI. Hum. Brain Mapp. 37, 20–34.

Ghosh, A., Rho, Y., McIntosh, A.R., Kötter, R., Jirsa, V.K., 2008. Noise during rest enables the exploration of the brain's dynamic repertoire. PLoS Comput. Biol. 4 e1000196.

Glasser, M.F., Sotiropoulos, S.N., Wilson, J.A., Coalson, T.S., Fischl, B., Andersson, J.L., Xu, J., Jbabdi, S., Webster, M., Polimeni, J.R., 2013. The minimal preprocessing pipelines for the Human Connectome Project. Neuroimage 80, 105–124.

Gong, G., He, Y., Concha, L., Lebel, C., Gross, D.W., Evans, A.C., Beaulieu, C., 2009. Mapping anatomical connectivity patterns of human cerebral cortex using in vivo diffusion tensor imaging tractography. Cereb. cortex 19, 524–536.

Goñi, J., van den Heuvel, M.P., Avena-Koenigsberger, A., de Mendizabal, N.V., Betzel, R.F., Griffa, A., Hagmann, P., Corominas-Murtra, B., Thiran, J.-P., Sporns, O., 2014. Resting-brain functional connectivity predicted by analytic measures of network communication. Proc. Natl. Acad. Sci. Unit. States Am. 111, 833–838.

Hellyer, P.J., Scott, G., Shanahan, M., Sharp, D.J., Leech, R., 2015. Cognitive flexibility through metastable neural dynamics is disrupted by damage to the structural connectome. J. Neurosci. 35, 9050–9063.

Hernández, M., Guerrero, G.D., Cecilia, J.M., García, J.M., Inuggi, A., Jbabdi, S., Behrens, T.E.J., Sotiropoulos, S.N., 2013. Accelerating fibre orientation estimation from diffusion weighted magnetic resonance imaging using GPUs. PLoS One 8 e61892.

Hillebrand, A., Barnes, G.R., Bosboom, J.L., Berendse, H.W., Stam, C.J., 2012. Frequency-dependent functional connectivity within resting-state networks: an atlas-based MEG beamformer solution. Neuroimage 59, 3909–3921.

Hillebrand, A., Tewarie, P., Van Dellen, E., Yu, M., Carbo, E.W.S., Douw, L., Gouw, A.A., Van Straaten, E.C.W., Stam, C.J., 2016. Direction of information flow in large-scale resting-state networks is frequency-dependent. Proc. Natl. Acad. Sci. Unit. States Am. 113, 3867–3872.

Hipp, J.F., Hawellek, D.J., Corbetta, M., Siegel, M., Engel, A.K., 2012. Large-scale cortical correlation structure of spontaneous oscillatory activity. Nat. Neurosci. 15, 884–890.

Honey, C.J., Sporns, O., Cammoun, L., Gigandet, X., Thiran, J.-P., Meuli, R., Hagmann, P., 2009. Predicting human resting-state functional connectivity from structural connectivity. Proc. Natl. Acad. Sci. Unit. States Am. 106, 2035–2040.

Hunt, B.A.E., Tewarie, P.K., Mougin, O.E., Geades, N., Jones, D.K., Singh, K.D., Morris, P.G., Gowland, P.A., Brookes, M.J., 2016. Relationships between cortical myeloarchitecture and electrophysiological networks. Proc. Natl. Acad. Sci. Unit. States Am. 113, 13510–13515.

Jansen, B.H., Rit, V.G., 1995. Electroencephalogram and visual evoked potential generation in a mathematical model of coupled cortical columns. Biol. Cybern. 73, 357–366.

Jbabdi, S., Sotiropoulos, S.N., Savio, A.M., Graña, M., Behrens, T.E.J., 2012. Model-based analysis of multishell diffusion MR data for tractography: how to get over fitting problems. Magn. Reson. Med. 68, 1846–1855.

Larson-Prior, L.J., Oostenveld, R., Della Penna, S., Michalareas, G., Prior, F., Babajani-Feremi, A., Schoffelen, J.-M., Marzetti, L., de Pasquale, F., Di Pompeo, F., 2013.

Adding dynamics to the human connectome project with MEG. Neuroimage 80, 190–201.
López, M.E., Engels, M., van Straaten, E.C.W., Bajo, R., Delgado, M.L., Scheltens, P., Hillebrand, A., Stam, C.J., Maestú, F., 2017. MEG beamformer-based reconstructions of functional networks in mild cognitive impairment. Front. Aging Neurosci. 9, 107.
Mehta-Pandejee, G., Robinson, P.A., Henderson, J.A., Aquino, K.M., Sarkar, S., 2017. Inference of direct and multistep effective connectivities from functional connectivity of the brain and of relationships to cortical geometry. J. Neurosci. Methods 283, 42–54.
Meier, J., Tewarie, P., Hillebrand, A., Douw, L., van Dijk, B.W., Stufflebeam, S.M., Van Mieghem, P., 2016. A mapping between structural and functional brain networks. Brain Connect. 6, 298–311.
Nolte, G., 2003. The magnetic lead field theorem in the quasi-static approximation and its use for magnetoencephalography forward calculation in realistic volume conductors. Phys. Med. Biol. 48, 3637.
O'Neill, G.C., Tewarie, P., Vidaurre, D., Liuzzi, L., Woolrich, M.W., Brookes, M.J., 2017. Dynamics of large-scale electrophysiological networks: a technical review. Neuroimage 180, 559–576.
Ranasinghe, K.G., Hinkley, L.B., Beagle, A.J., Mizuiri, D., Honma, S.M., Welch, A.E., Hubbard, I., Mandelli, M.L., Miller, Z.A., Garrett, C., 2017. Distinct spatiotemporal patterns of neuronal functional connectivity in primary progressive aphasia variants. Brain 140, 2737–2751.
Robinson, S.E., 1999. Functional neuroimaging by synthetic aperture magnetometry (SAM). Recent Adv. Biomagn. 302–305.
Robinson, P.A., 2012. Interrelating anatomical, effective, and functional brain connectivity using propagators and neural field theory. Phys. Rev. E 85, 11912.
Robinson, P.A., Zhao, X., Aquino, K.M., Griffiths, J.D., Sarkar, S., Mehta-Pandejee, G., 2016. Eigenmodes of brain activity: neural field theory predictions and comparison with experiment. Neuroimage 142, 79–98.
Roxin, A., Brunel, N., Hansel, D., 2005. Role of delays in shaping spatiotemporal dynamics of neuronal activity in large networks. Phys. Rev. Lett. 94, 238103.
Saggio, M.L., Ritter, P., Jirsa, V.K., 2016. Analytical operations relate structural and functional connectivity in the brain. PLoS One 11 e0157292.
Seymour, R.A., Wang, H., Rippon, G., Kessler, K., 2018. Oscillatory networks of high-level mental alignment: a perspective-taking MEG study. Neuroimage 177, 98–107. https://doi.org/10.1016/j.neuroimage.2018.05.016.
Smith, R.E., Tournier, J.-D., Calamante, F., Connelly, A., 2015. The effects of SIFT on the reproducibility and biological accuracy of the structural connectome. Neuroimage 104, 253–265.
Sotiropoulos, S.N., Zalesky, A., 2017. Building connectomes using diffusion MRI: why, how and but. NMR Biomed., e3752 (ahead of print).
Sotiropoulos, S.N., Jbabdi, S., Xu, J., Andersson, J.L., Moeller, S., Auerbach, E.J., Glasser, M.F., Hernandez, M., Sapiro, G., Jenkinson, M., 2013. Advances in diffusion MRI acquisition and processing in the human connectome project. Neuroimage 80, 125–143.
Sotiropoulos, S.N., Hernández-Fernández, M., Vu, A.T., Andersson, J.L., Moeller, S., Yacoub, E., Lenglet, C., Ugurbil, K., Behrens, T.E.J., Jbabdi, S., 2016. Fusion in diffusion MRI for improved fibre orientation estimation: an application to the 3T and 7T data of the Human Connectome Project. Neuroimage 134, 396–409.
Stam, C.J., 2014. Modern network science of neurological disorders. Nat. Rev. Neurosci. 15, 683–695.
Stam, C.J., Tewarie, P., Van Dellen, E., Van Straaten, E.C.W., Hillebrand, A., Van Mieghem, P., 2014. The trees and the forest: characterization of complex brain networks with minimum spanning trees. Int. J. Psychophysiol. 92, 129–138.
Tewarie, P., Hillebrand, A., van Dellen, E., Schoonheim, M.M., Barkhof, F., Polman, C.H., Beaulieu, C., Gong, G., van Dijk, B.W., Stam, C.J., 2014. Structural degree predicts functional network connectivity: a multimodal resting-state fMRI and MEG study. Neuroimage 97, 296–307.
Tewarie, P., Bright, M.G., Hillebrand, A., Robson, S.E., Gascoyne, L.E., Morris, P.G., Meier, J., Van Mieghem, P., Brookes, M.J., 2016a. Predicting haemodynamic networks using electrophysiology: the role of non-linear and cross-frequency interactions. Neuroimage 130, 273–292.
Tewarie, P., Hillebrand, A., van Dijk, B.W., Stam, C.J., O'Neill, G.C., Van Mieghem, P., Meier, J.M., Woolrich, M.W., Morris, P.G., Brookes, M.J., 2016b. Integrating cross-frequency and within band functional networks in resting-state MEG: a multi-layer network approach. Neuroimage 142, 324–336.
Tewarie, P., Hunt, B.A.E., O'Neill, G.C., Byrne, A., Aquino, K., Bauer, M., Mullinger, K.J., Coombes, S., Brookes, M.J., 2018. Relationships between neuronal oscillatory amplitude and dynamic functional connectivity. Cerebr. Cortex 1–14 (ahead of print).
Tzourio-Mazoyer, N., Landeau, B., Papathanassiou, D., Crivello, F., Etard, O., Delcroix, N., Mazoyer, B., Joliot, M., 2002. Automated anatomical labeling of activations in SPM using a macroscopic anatomical parcellation of the MNI MRI single-subject brain. Neuroimage 15, 273–289.
Van Essen, D.C., Smith, S.M., Barch, D.M., Behrens, T.E.J., Yacoub, E., Ugurbil, K., Consortium, W.-M.H.C.P., 2013. The Wu-Minn human connectome project: an overview. Neuroimage 80, 62–79.
Visser, S., Nicks, R., Faugeras, O., Coombes, S., 2017. Standing and travelling waves in a spherical brain model: the Nunez model revisited. Phys. Nonlinear Phenom. 349, 27–45.
Wang, M.B., Owen, J.P., Mukherjee, P., Raj, A., 2017. Brain network eigenmodes provide a robust and compact representation of the structural connectome in health and disease. PLoS Comput. Biol. 13 e1005550.
Wilson, H.R., Cowan, J.D., 1972. Excitatory and inhibitory interactions in localized populations of model neurons. Biophys. J. 12, 1–24.